JOURNAL OF Materials CHEMISTRY

Thermal evolution of cobalt hydroxides: a comparative study of their various structural phases

Z. P. Xu and H. C. Zeng*

Department of Chemical Engineering, Faculty of Engineering, National University of Singapore, 10 Kent Ridge Crescent, Singapore 119260. E-mail: chezhc@nus.edu.sg

Received 23rd June 1998, Accepted 11th August 1998

Through an atmosphere-controlled method, a new phase of hydrotalcite-like Co hydroxide with mixed valent states has been synthesised, along with preparations of known α and β phases. Structural and thermal behaviours of all the Co hydroxides have been compared. Three major stages of decomposition are found: (i) 149–164 °C for dehydration of interlayer water, (ii) 185–197 °C and (iii) 219–222 °C for dehydroxylation of hydrotalcite- and brucite-like phases, respectively. Intercalated nitrate anions in hydrotalcite-like phases decompose largely during stage (ii). The oxide Co_3O_4 starts to form at temperatures as low as 165 °C especially for hydrotalcite-like phases. An intermediate compound, $HCoO_2$, which is formed thermally, decomposes at 258–270 °C. The Co_3O_4 oxide converts into CoO at 842–858 and 935–948 °C respectively in nitrogen and air, which is much lower than the previously reported range of 1000–1200 °C. Surface areas of calcined samples are found to be proportional to the intercalated anion content. The catalytic activity of the resultant Co_3O_4 oxides with nitrous oxide is 7.2–8.2 mmol N_2O g^{-1} h^{-1} at 375 °C, which is comparable to some reported active catalyst systems.

Introduction

In recent years, divalent transition metal hydroxides including their double hydroxides with trivalent *p* block (AIII) or *d* block metals have received increasing attention owing to their unique physico-chemical properties for electrochemical, magnetic and catalytic applications.[1–8]

One of the common features for this class of materials is their layered structure.[9,10] A divalent metal cation is located in the center of the octahedron formed by six hydroxyl groups. The metal-octahedra then share edges to form two-dimensionally infinite sheets, which is similar to the basic structure of brucite [$Mg(OH)_2$].[9,10] The brucite-like sheets can stack upon each other to build a three-dimensional network according to various chemical interactions (mainly hydrogen bonding) between the sheets.[9,10] It has been well known for layered double hydroxides (LDH) that when some of the divalent d block metal cations are substituted by a trivalent cation, a positive charge is generated in the brucite-like sheet. To restore overall charge neutrality of solid, the extra positive charge can be balanced by intercalating anion species into inter-brucite-like-sheet space, resulting in a hydrotalcite-like phase [HT; named after the mineral compound $Mg_6Al_2(OH)_{16}CO_3 \cdot 4H_2O$] in most cases.[9]

Nevertheless, the formation and structure of layered mono-transition metal hydroxides are not studied as explicitly as in LDH materials.[9,10] For example, it has long been known that there are two major types of nickel and cobalt hydroxides (α and β phases).[1–8] The structure for the latter form (β) has been identified as a brucite-like phase, but the former (α) has remained largely unknown regarding its actual formation mechanism. Among many speculative models proposed for the α phase formation,[1–5] two prominent models, 'hydroxyl vacancies' and 'mixed valent state' (with mixed M^{2+} and M^{3+}) appear plausible.[2,3] In particular, the 'hydroxyl vacancies' model has been experimentally confirmed very recently, which reveals that the nickel and cobalt are strictly in the oxidation state of 2+ while the missing OH^- groups in brucite-like sheets are compensated by intercalated anions.[8]

We have noted that most of these material syntheses are conducted in liquid phase under static atmospheric conditions. Thus, oxidation of divalent transition metal cations by oxygen in static air, if occurring, may not be severe because transport of oxygen to the liquid phase is limited by the gas–bulk-liquid interface. However, if air (and hence oxygen) is constantly supplied through bubbling to the liquid phase, the gas–liquid contact area can be significantly increased. The oxidation of $Co^{2+}(3d^7)$ to $Co^{3+}(3d^6)$ has been recently observed in our preparation of the LDH compound $Mg^{II}Co^{II}Co^{III}$-HT using a dynamic air-flow approach.[11] In this connection, without involvement of Mg^{II}, the possibility of fabricating a $Co^{II}Co^{III}$ hydrotalcite-like phase had been indicated in our previous synthesis of Mg–Co mixed oxide spinels.[12]

Here, we report a systematic investigation on preparation of Co hydroxide compounds using the dynamic gas-flow of either protective (nitrogen) or oxidative gas (air). In addition to formation of α and β phases, the oxidation of $Co^{2+}(3d^7)$ to $Co^{3+}(3d^6)$ occurs in the dynamic air-flow experiment, leading to generation of a new type of $Co^{II}Co^{III}$ hydrotalcite-like compound. Using the well defined starting compounds (α and β phases, along with the newly found $Co^{II}Co^{III}$ hydrotalcite-like phase), we are in a better position to conduct a comparative investigation on the thermal evolution of all these Co hydroxides, which has been unclear in the literature owing to insufficient materials characterization (such as metal oxidation state and anion content in the interlayer space) and lack of mechanistic understanding on material formation.[2,3,6–8,13] The study will also correlate thermal evolution with gaseous chemical constituents and chemical reactivity (an important index for catalytic application) of the thermally obtained end product Co_3O_4 using N_2O as a probe molecule.[14]

Experimental

Materials preparation

Two series of Co hydroxide samples (N1–N5 and A1–A6) with various structural phases (brucite and hydrotalcite-like and their mixtures) were prepared using an atmosphere-controlled precipitation method.[11] In the sample preparation, 20.0 ml of 1.0 M aqueous cobalt nitrate solution [$Co(NO_3)_2 \cdot 6H_2O$, >99.0%, Fluka] was added into 100 ml 0.5 M ammoniacal solution in a three-necked round-bottom

*Tel: +65 874 2896. Fax: +65 779 1936.

Table 1 Sample nomenclature and preparation conditions

Sample	Atmosphere	Addition time	Aging time	Structural phase[a]
N1	N_2	15 s	5 min	HT(II)
N2	N_2	15 s	2 h	HT(II)
N3	N_2	15 s	4 h	HT(II)+B(II)
N4	N_2	15 s	6 h	B(II)
N5	N_2	15 s	8 h	B(II)
A1	Air	4 min	3 min	B(II)+HT(II,III)
A2	Air	4 min	2 h	B(II)+HT(II,III)
A3	Air	4 min	4 h	HT(II,III)+B(II)
A4	Air	4 min	8 h	HT(II,III)+B(II)
A5	Air	4 min	16 h	HT(II,III)
A6	Air	4 min	24 h	HT(II,III)

[a]HT(II)=Co^{II} hydrotalcite-like phase [*i.e.*, α-$Co(OH)_2$]; B(II)=Co^{II} brucite-like phase [*i.e.*, β-$Co(OH)_2$]; HT(II,III)=$Co^{II}Co^{III}$ hydrotalcite-like phase; order of structural phase appears according to intensity of XRD data.

flask within a given time (Table 1) under stirring. The atmosphere for precipitation was controlled by bubbling the solution with either purified nitrogen (Soxal, O_2 <2 vpm) or purified air (Soxal, $O_2=21\pm1\%$, $H_2O<2$ vpm, and hydrocarbons <5 vpm) at a rate of 40 ml min^{-1} at room temperature. It should be noted that there are three preparative parameters (atmosphere, addition time, and aging time) varied in these experiments (Table 1). The final pH values of the filtrate were in the range 8.5–8.2 depending on the addition/aging time in the experiment.

Materials characterisation

Crystallographic information on the precipitates was investigated by X-ray powder diffraction (XRD). The XRD patterns with diffraction intensity *versus* 2θ were recorded in a Shimadzu XRD-6000 X-ray diffractometer with Cu-Kα radiation ($\lambda=1.5418$ Å) from 8–40° at a scanning speed of 3° min^{-1}. Chemical bonding of cobalt–oxygen, hydroxyl and some anions (mainly nitrate) was studied by FTIR (Shimadzu FTIR-8101) using the potassium bromide (KBr) pellet technique. The spectra were measured with a resolution of 2 cm^{-1} and 100 scans were accumulated. Elemental analysis (EA) for nitrogen and carbon contents in the as-precipitated samples was performed using a Perkin Elmer 2400 CHN elemental analyzer. Cobalt content in the precipitate samples was determined by thermogravimetric analysis (TGA, Shimadzu TGA-50) based on the end products Co_3O_4 at 600 and CoO at 950 °C. The trivalent cobalt content in some important precipitates (N1, N5, A1 and A6) was determined by a redox titration method in which 10.00 mg of solid sample were dissolved in 20.0 ml 1.0 M HCl solution upon gentle heating. The produced Cl_2 was gradually purged with N_2 (60 ml min^{-1}) and passed through a 50.0 ml 0.01 M KI solution mixed with starch indicator. The resultant blue mixture was then titrated against a $Na_2S_2O_3$ solution (0.0100 M) until disappearance of the blue coloration.

Differential scanning calorimetry (DSC, Netzsch DSC200), differential thermal analysis (DTA, Shimadzu DTA-50), and thermogravimetric analysis (TGA, Shimadzu TGA-50) studies were carried out with various gas backgrounds in order to understand the thermal evolution of the prepared cobalt hydroxides. Samples in DSC measurements were heated from 40–400 °C at a rate of 10 °C min^{-1} under nitrogen with a gas flow rate of 15 ml min^{-1}. To differentiate thermal processes at various heating stages, FTIR spectra were recorded for samples that were heated to a specified temperature in DSC measurements. In DTA measurements, the heating/cooling rate was kept the same as in DSC, but with air gas-flow at 60 ml min^{-1} and with nitrogen gas-flow at 100 ml min^{-1}, respectively. To further explain the DSC/DTA results, TGA measurements were carried out from 50–950 °C (at two heating rates: 10 °C min^{-1} for 50–900 °C and 2 °C min^{-1} for 900–950 °C) with an air flow at 60 ml min^{-1}.

The as-prepared precipitates were also heat-treated at 200, 300 and 400 °C, respectively, for 2 h with static laboratory air in an electric furnace (Carbolite). Specific surface areas were determined by a multi-point BET method using a Nova-1000 Instrument. Prior to N_2 adsorption–desorption measurement, each sample was degassed with N_2 purge for 3 h at a temperature lower than its respective heat-treated temperature.

In catalytic activity tests, 150 mg of 40–60 mesh sample calcined at 400 °C (2 h) were used in a tubular quartz reactor (inner diameter=0.4 cm, $V=0.088$ cm^3) in each run. In a typical experiment, N_2O gas (1 mol%, balanced with He) was fed at a rate of 30 ml min^{-1} (F) through the catalyst bed (GHSV=20 500 h^{-1}). The GHSV was also increased to 41 000, 61 500, and 82 000 h^{-1} to investigate the effect of feed rate on the catalytic activity. The outlet gases, cooled in a coil, were analyzed by gas chromatography (GC) on a Perkin-Elmer AutoSystem-XL (TCD detector) using a 4 ft Porapak Q (80/100 mesh) column. The oven temperature of GC was maintained at 120 °C, and the flow rate of He carrier gas was 40 ml min^{-1}. The catalytic activity for N_2O decomposition was evaluated in terms of conversion percentage, $X=(P_{i,N_2O}-P_{f,N_2O})/(P_{i,N_2O}+0.5P_{i,N_2O}P_{f,N_2O})$, where P_{i,N_2O} and P_{f,N_2O} are inlet and outlet partial pressures of nitrous oxide.[15,16]

Results and discussion

Preparation of Co hydroxides with designed phases

In this work, three preparative parameters (atmosphere, addition time, and aging time) were varied. As indicated in Table 1, two different hydrotalcite-like phases and one pure brucite-like phase or their mixtures can be obtained using an appropriate combination of these parameters. Fig. 1 shows some representative XRD patterns which indicate that the synthesis atmosphere gives a greater influence on crystallographic structure of the resulting precipitates.

In a nitrogen atmosphere, an α phase precipitate can be obtained upon fast addition and short aging (N1, Table 1). EA investigation reveals that there is no trivalent cobalt but there is anion intercalation in this phase (Table 2). On the

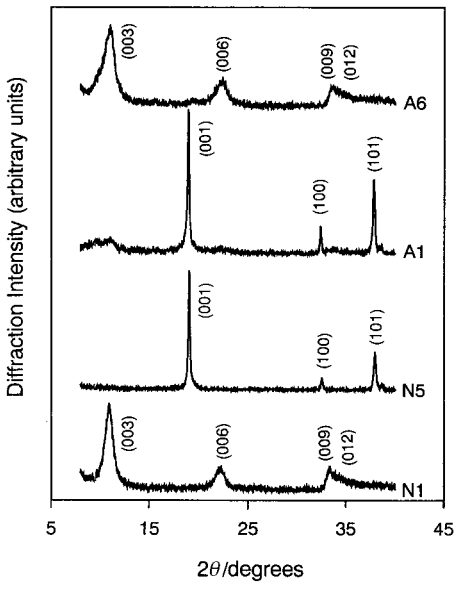

Fig. 1 Representative XRD patterns for as-prepared Co hydroxides: N1, N5, A1, and A6, noting that major diffraction peaks of the samples are located in the reported 2θ range.

Table 2 Elemental analysis and TGA results for some representative samples

Sample	$[Co^{3+}]/[Co]^a$	$[NO_3^- + 2CO_3^{2-}]/[Co]^b$	Structural phase[c]	L1 (%)[d]	L2 (%)	L3 (%)
N1	0	0.19	HT(II)	8.9	11.8	4.6
N5	0	0.02	B(II)	0.8	9.1	4.6
A1	0.04	0.13	B(II)+HT(II,III)	3.6	13.4	4.0
A6	0.28	0.32	HT(II,III)	8.0	16.5	4.7

Sample	Co (%)	NO_3^- (%)	CO_3^{2-} (%)	H_2O (%)	Chemical formula
N1	55.2	6.6	2.1	10.9	$Co^{II}(OH)_{1.81}(NO_3)_{0.11}(CO_3)_{0.04}\cdot 0.65H_2O$
N5	63.1	0	0	0.5	$Co^{II}(OH)_2\cdot 0.03H_2O$
A6	52.0	14.0	1.5	5.1	$Co^{II}_{0.72}Co^{III}_{0.28}(OH)_{1.96}(NO_3)_{0.26}(CO_3)_{0.03}\cdot 0.3H_2O$

[a]Mole ratio of trivalent cobalt to total cobalt in the precipitate samples. [b]Mole ratio of total charges of anion species to total cobalt in the precipitate samples; CO_3^{2-} results from ambient CO_2 dissolution. [c]The phase notation is the same as in Table 1. [d]L1, L2 and L3 are weight loss percentages from 40–160 °C, 160–230 °C, and 230–500 °C.

basis of XRD/EA/TGA studies, the precipitate (N1) of the hydrotalcite-like phase has an inter-brucite-like-sheet distance of 8.09 Å, and a chemical formula $Co^{II}(OH)_{1.81}(NO_3)_{0.11}(CO_3)_{0.04}\cdot 0.65H_2O$. In contrast, a sample similarly prepared in nitrogen but with a longer aging time is a pure brucite-like compound (N5, Fig. 1). Again, cobalt is strictly divalent and there are virtually no anions or water intercalated in this compound. The inter-brucite-like-sheet distance determined by XRD is 4.66 Å, which is identical to the literature data for the β phase.[17] From N1 to N5 (Table 1) the sequential evolution from $Co^{II}(OH)_{1.81}(NO_3)_{0.11}(CO_3)_{0.04}\cdot 0.65H_2O$ to $Co^{II}(OH)_2$ can be conducted by changing the aging time. A two-phase material is seen in sample N3 in which both $Co^{II}(OH)_{1.81}(NO_3)_{0.11}$ $(CO_3)_{0.04}\cdot 0.65H_2O$ and $Co^{II}(OH)_2$ are present.

The above Co^{II} hydrotalcite-like to Co^{II} brucite-like transformation occurs under a protective atmosphere of nitrogen. However this transformation can be steered in the reverse direction when nitrogen is replaced by air. A predominant brucite-like phase can be prepared within 4 min (A1, Table 1 and 2, Fig. 1). Surprisingly, this newly formed brucite-like phase can be transformed into a pure hydrotalcite-like phase upon prolonged aging in air. As demonstrated in the A1–A6 series, bi-phasic mixtures are observed in A1–A4 while hydrotalcite-like compounds are found in A5 and A6. Related to this phase evolution, the Co^{3+} to total cobalt ratio is increased from 0.04 to 0.28 from the sample A1 to A6 (Table 2) and about 30% of initial Co^{2+} has been oxidized to Co^{3+} in A5 and A6. In response to the increase in positive charge, a similar amount of negative anionic species is found in the interlayer space (*i.e.*, 0.28 *vs.* 0.32 determined for A6; Table 2). The chemical formula for both A5 and A6 is thus $Co^{II}_{0.72}Co^{III}_{0.28}(OH)_{1.96}(NO_3)_{0.26}(CO_3)_{0.03}\cdot 0.3H_2O$ according to XRD/EA studies and the inter-brucite-like sheet distance for this compound is 7.98 Å.

In view of the above results, Co hydroxides can apparently be tailor-made with a desired structure and chemical composition, including electronic configuration for the cations, using the current approach.

Thermal decomposition of Co hydroxides

Fig. 2 shows results of DSC investigations on the nitrogen-precipitated samples N1–N5. Low-temperature endothermic humps at *ca.* 130 °C in N1–N3 can be assigned to depletion of surface adsorbed water, while bands at 149–158 °C can be attributed to the release of interlayer water molecules.[18–20] Collapse of the hydrotalcite-like structure is observed at *ca.* 190–195 °C for N1–N4 (only a small shoulder in N4, *i.e.*, a trace phase of HT). Finally large endothermic bands at 219–222 °C in N4 and N5 can be assigned unambiguously to decomposition of the brucite-like structure, which normally occurs at a higher temperature.[18–20] Similar to the structural

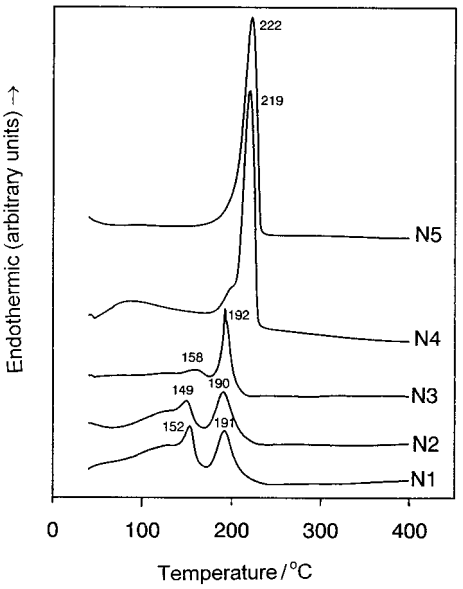

Fig. 2 DSC curves for the sample series prepared under nitrogen atmosphere: N1–N5.

evolution revealed by XRD, a smooth transition from the hydrotalcite to brucite-like phase can be seen from these DSC curves.

DSC scans for air-prepared samples A1–A6 are shown in Fig. 3. As can be seen, thermal events corresponding to depletion of the interlayer water and dehydroxylation of hydrotalcite-like structure take place at *ca.* 152–164 °C (first peak) and 185–197 °C (second peak) respectively, in all samples. In good agreement with the XRD results, which show a predominant brucite-like phase and a small hydrotalcite-like phase in A1 and A2 (Table 1), the DSC investigation in Fig. 3 also indicates the co-existence of the two phases. Compared to hydrotalcite-like phase, the brucite-like phase is thermally more stable. The third endothermic effect (217–219 °C) due to dehydroxylation of the brucite-like structure is observed in A1 and A2. The endothermic effect observed at *ca.* 258 °C in A5 will be explained below.

It is noted that thermal behaviours of N1 and A6 considerably differ (Fig. 2 and 3), although they both have hydrotalcite-like structures (Fig. 1). In view of the absence of trivalent cations, the Co^{II} hydrotalcite-like structure in N1 (α phase; $Co^{II}(OH)_{1.81}(NO_3)_{0.11}(CO_3)_{0.04}\cdot 0.65H_2O$) can be described well by the 'hydroxyl group deficiencies' model.[2,8] By contrast, the $Co^{II}Co^{III}$ hydrotalcite-like phase in A6 ($Co^{II}_{0.72}Co^{III}_{0.28}(OH)_{1.96}(NO_3)_{0.26}(CO_3)_{0.03}\cdot 0.3H_2O$) can be ascribed to formation of common hydrotalcite-like phase that contains both divalent and trivalent cations due to the partial

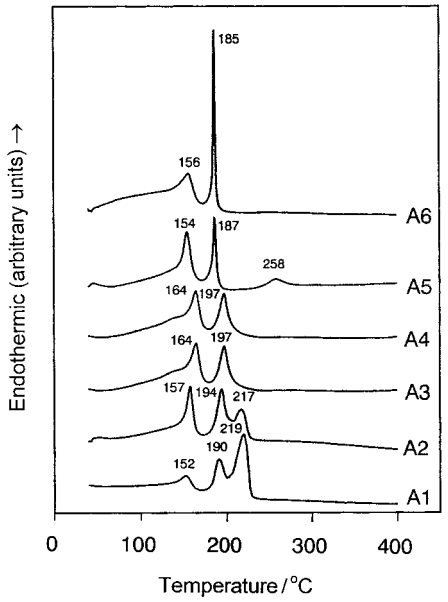

Fig. 3 DSC curves for the sample series prepared under air atmosphere: A1–A6.

oxidation of Co^{2+}. The speculated 'mixed valent state' model[3] can be thus confirmed. With respect to the formation mechanism, the increase in peak intensity and sharpness in A6 (second peak, Fig. 3) reflects an increase in interaction between cations and intercalated anions due to presence of trivalent cobalt. More anionic species are found in the $Co^{II}Co^{III}$ hydrotalcite-like phase than in the Co^{II} HT-like phase (0.32 in A6 *vs.* 0.19 in N1; Table 2). It is thus believed that stronger electrostatic attraction would lead to a more intense endothermic effect observed during the dehydroxylation.

Thermal evolution to Co_3O_4 oxides

Owing to structural and chemical differences, different thermal evolution behaviours and thermal stability of the Co hydroxides are expected upon heat-treatment. Fig. 4(a) shows FTIR spectra for the stage-calcined N1 sample (see Experimental section). As can be seen, fingerprint IR absorptions at 580 and 660 cm^{-1} for the Co_3O_4 spinel phase are fully developed after heat-treatment at 165 °C.[12] Upon the lowering of intensities for hydroxyl group and intercalated nitrate ion bands at 3430 cm^{-1} and 1384 and 839 cm^{-1},[21–23] the metal-oxygen vibrational absorption modes at 564–580 and 660 cm^{-1} increase markedly.[9,24] Fig. 4(b) shows in FTIR spectra the metal–OH vibration of the A1 sample at *ca.* 494 cm^{-1},[9,24] after heat-treatment at 165 °C. It is thus confirmed that sample A1 is thermally more stable than N1. Furthermore, the hydroxyl group (3630 cm^{-1}) in the brucite-like phase is still very pronounced at this temperature and it is only significantly reduced at around 200 °C when dehydroxylation commences. It should be noted that, regardless of types of initial precipitates, the final decomposed products of N1 and A1 at higher temperatures are exclusively in the spinel form (IR bands at 564 and 660 cm^{-1} for Co_3O_4).[12] The oxidative formation of Co_3O_4 phase is completed with precipitation of nitrate anion, in the absence of ambient oxygen. In this connection, a small peak at 1270 cm^{-1} for N1 heated to 190 °C can be assigned to the asymmetric vibration of monodentate nitrate ion [asymmetric vibration mode: $\nu_{as}(ONO_2)$].[20,25] Nitrate ion evolution during heating can be seen clearly in A6 [Fig. 4(c)] that contains the largest amount of anions (Table 2). In addition to the formation of monodentate species [1310 cm^{-1} for the $\nu_{as}(ONO_2)$ and 1470 cm^{-1} for the symmetric vibration mode $\nu_s(ONO_2)$] [20,25] at 165 °C, the nitrate anion also undergoes a symmetry-lowering from a flat-laying configuration (1384 and 839 cm^{-1}: ν_3 and ν_2 modes of NO_3^- with D_{3h} symmetry) to a tilted or vertical position, which is indicated by a newly emerging peak at 1010 cm^{-1} (ν_1 mode of NO_3^-) of C_{2v} symmetry.[21,22,26]

Although the final calcined products are all Co_3O_4, thermal evolution paths may differ considering the substantial differences of starting materials in chemical composition, oxidation state, and molecular structure (Table 2). To differentiate the decomposition paths, the formation process of Co_3O_4 was further investigated by DTA using nitrogen and air. Fig. 5 shows DTA results for N1–N5; decomposition processes in nitrogen are quite similar to those in DSC (Fig. 2) in which nitrogen was also used. However, the thermal behaviour changes considerably in air-DTA experiments. For example, exothermic peaks at 172 °C (N5) and 189 °C (N4) can be attributed to Co^{2+} oxidation to Co^{3+} in the brucite-like phase. The peaks are still exothermic even considering the decomposition (which is endothermic): [27]

$$3\ Co(OH)_2 + 1/2\ O_2 \rightleftharpoons Co_3O_4 + 3\ H_2O$$
$$\Delta H_r^\circ = -25\ kJ\ mol^{-1}\ Co_3O_4 \qquad (1)$$

For the A1–A6 series shown in Fig. 6, the endothermic peaks at 211 °C (A1) and 206 °C (A2) observed in nitrogen atmosphere can be assigned to the decomposition of a mixed brucite-like phase. Nevertheless, this endothermic effect is cancelled out by the exothermic oxidation of the brucite-like phase for the same samples measured in air (A1 and A2, Fig. 6).

Following the DSC /XRD /FTIR /DTA results, weight losses before 500 °C in TGA can be broadly classified into three major types (L1, L2 and L3; Table 2). The first, between 40 and 160 °C can be ascribed to dehydration of samples (surface and/or interlayer water). This assignment is supported by the fact that a negligible loss is observed for the essentially brucite-like phase N5 while larger weight losses are seen for all hydrotalcite-like samples (N1 > A6 > A1 ≫ N5; Table 2). The second stage between 160 and 230 °C is attributed to dehydroxylation of Co hydroxides, as all samples exhibit the largest losses over this temperature range. The final stage between 230 and 500 °C can be ascribed to a continued decomposition process for large-sized particles (mass transport limiting) and a decomposition of $HCo^{III}O_2$.

According to TGA all samples show a small weight loss between 270 and 274 °C within the total L3. However, this loss becomes much more pronounced in samples A4 and A5 with a total loss L3 of 7.3% and 7.1%, respectively, compared to L3 = 4.0–4.7% in Table 2. The weight losses at 270–274 °C correspond to the endothermic peaks at 262–270 °C found in the DTA scans of A4 and A5 (Fig. 6; and similarly observed in the DSC scan of A5, Fig. 3), which can be assigned to decomposition of cobalt oxide hydroxide [$HCo^{III}O_2$]. This trivalent Co compound also has a hexagonal-layered structure, layers of which are bonded to each other by hydrogen bonding and decomposes in the same temperature range under vacuum or oxygen atmosphere: [28]

$$12\ HCoO_2 \rightleftharpoons 4\ Co_3O_4 + 6\ H_2O + O_2 \qquad (2)$$

It has been established thermogravimetrically that in the temperature range 120–190 °C trivalent Co hydroxide first forms $HCoO_2$ before being converting to Co_3O_4 at 240–300 °C.[13,28] Furthermore $HCoO_2$ can also be oxidatively prepared in an ambient atmosphere *via* oxidation of β-$Co(OH)_2$.[28] Since the TGA measurements were conducted with air, divalent cobalt can be oxidised to the trivalent $HCoO_2$ on heating.

The pronounced $HCoO_2$-decomposition for the A4 and A5 samples in TGA/DTA/DSC can be attributed to the presence of trivalent cobalt plus the on-site formed $HCoO_2$. However, $HCoO_2$ decomposition is not observable in DTA/DSC

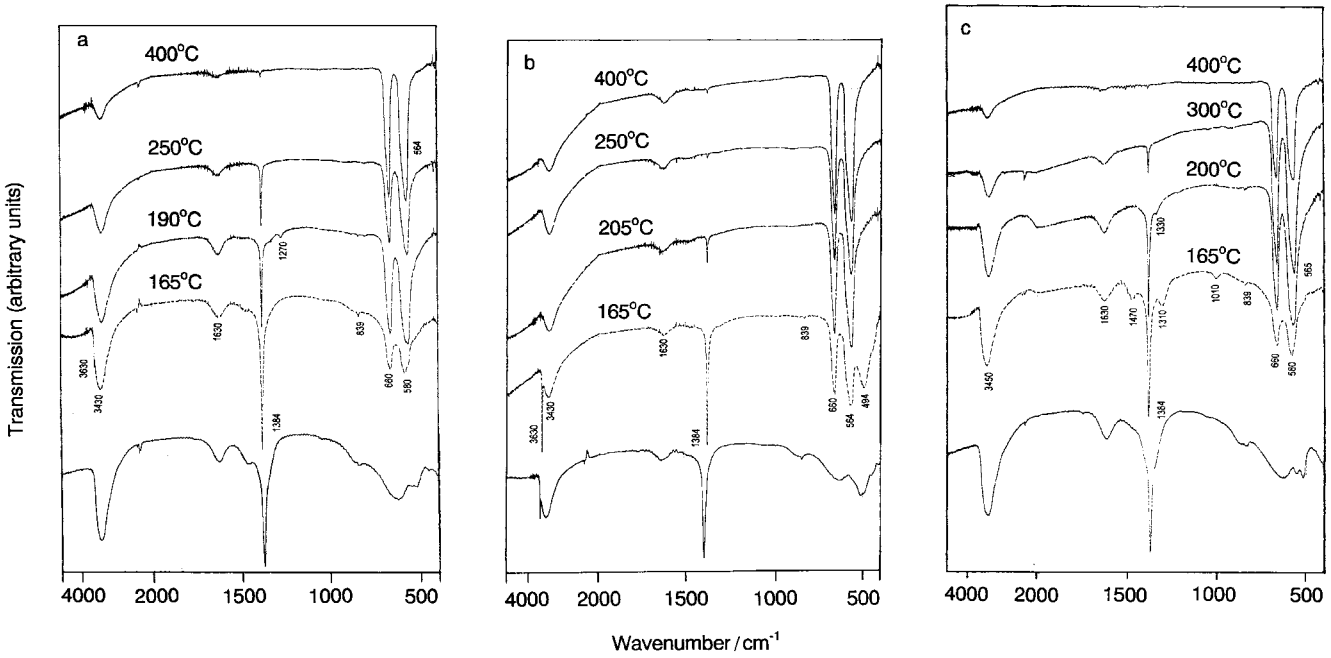

Fig. 4 FTIR spectra for three as-prepared samples: (a) N1, (b) A1, and (c) A6 after heating from room temperature (unmarked) to the temperatures (marked) of some major thermal events in the DSC scans (10 °C min^{-1} in nitrogen).

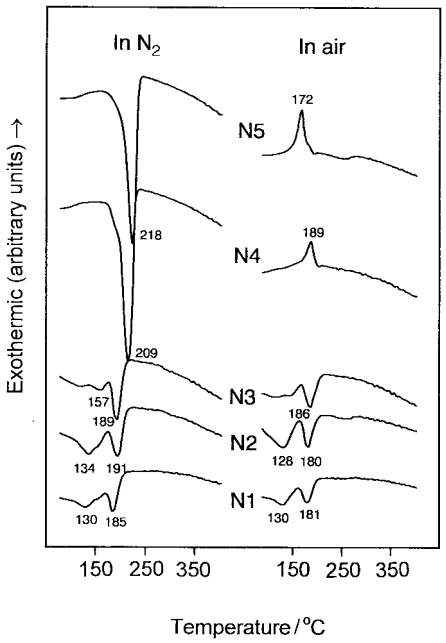

Fig. 5 DTA curves for N1–N5 sample series measured under nitrogen and air atmospheres.

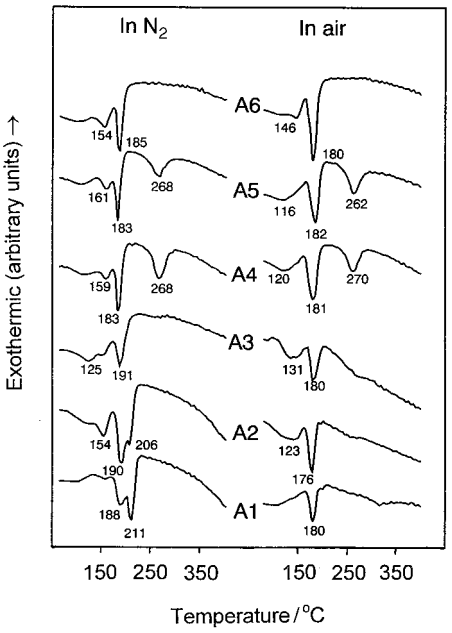

Fig. 6 DTA curves for A1–A6 sample series measured under nitrogen and air atmospheres.

measurements for A6 even though it contains trivalent cobalt. This difference can be related to distribution homogeneity of trivalent cobalt in the precipitates. Compared to the A5 sample, the second endothermic peak of the DSC-scan for A6 (Fig. 3 and similarly in DTA scans of Fig. 6) is much sharper. This is also observed for other well aged samples (>24 h, not listed in Table 1). As mentioned earlier, the sharpness of DSC peak indicates a well defined phase. The above observations lead to our belief that a more homogeneous distribution of trivalent cobalt cations among the divalent ions leads to a dimunition of the $HCoO_2$ phase.

Based on the TGA data, it can be concluded that the anionic species decompose almost simultaneously with dehydroxylation of the Co hydrotalcites (N1, A1 and A6; Table 2) in stage two, since the losses (L3) at stage three are essentially the same for all samples including the anion-free N5. This view is further supported by FTIR studies in Fig. 4(a)–(c) which show a significant reduction in the nitrate ion absorption at 1384 cm^{-1} over this temperature range.

Transformation between Co_3O_4 and CoO

It is known that Co_3O_4 is a thermodynamically stable form under an oxygen containing atmosphere. The stability of the prepared Co_3O_4 was examined under inert gas (nitrogen) or an oxygen-containing atmosphere (air). DTA investigation on decomposition and restoration of Co_3O_4 during heating-cooling cycles is shown in Fig. 7 and 8. The endothermic peaks at *ca.* 846–858 °C for samples N1–N5 heated under nitrogen (Fig. 7) can be described by the forward reaction of the

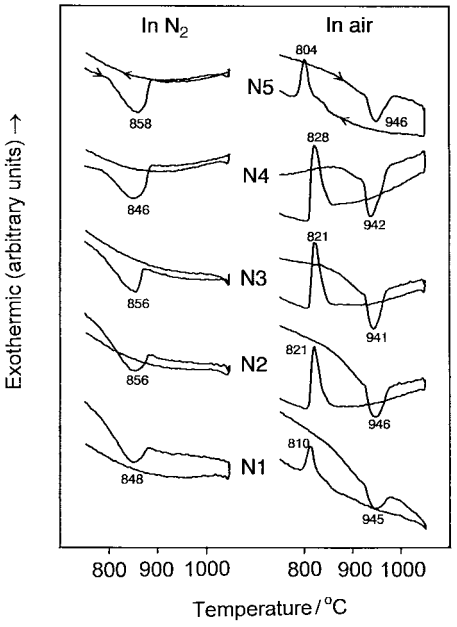

Fig. 7 DTA heating-cooling cycles for N1–N5 sample series measured under nitrogen and air atmospheres; arrows indicate the heating–cooling directions.

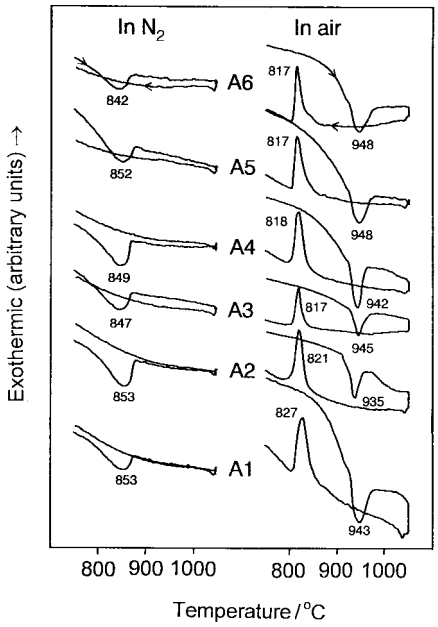

Fig. 8 DTA heating–cooling cycles for A1–A6 sample series measured under nitrogen and air atmospheres; arrows indicate the heating–cooling directions.

following chemical equilibrium:

$$Co_3O_4 \rightleftharpoons 3\ CoO + 1/2\ O_2 \qquad (3)$$

However, this decomposition occurs at a much higher temperature (941–946 °C) for the same series under air. As it is reversible, the above reaction shifts to the left when the temperature is lowered and there is sufficient oxygen in the gaseous phase [$P_{O_2} = 2.1 \times 10^4$ Pa using air at this experimental setting (total pressure = 1 atm)]. As indicated by the large exothermic peaks at 804–828 °C (Fig. 7), the reverse reaction of eqn. (3) is exothermic due to oxidation of divalent cobalt.[29] A similar observation is seen for the sample series A1–A6 in Fig. 8 over the same heating–cooling range. Since there is no oxygen, the reverse transition is not observed in the DTA experiments using nitrogen (Fig. 7 and 8).

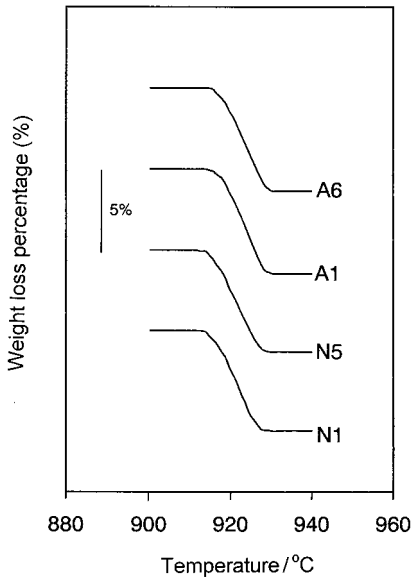

Fig. 9 TGA curves for some selected Co hydroxides during $Co_3O_4 \rightleftharpoons 3\ CoO + 1/2\ O_2$ phase transformation.

The observed similar DTA-heating–cooling cycles for both sets of samples indicate that all Co hydroxides should have similar chemical constituents over the temperature range studied. This point has been further confirmed with the TGA investigation shown in Fig. 9. In good agreement with the DTA results, there is no further weight loss at temperature >500 °C until the Co_3O_4 phase decomposes. Conversion of Co_3O_4 to CoO occurs at >910 °C (note: a slow heating rate of 2 °C min^{-1} is used). The detected weight loss is in the range of 6.23–6.46%, very close to the theoretical value of 6.62% according to eqn. (3). On the basis of DTA/TGA results, the Co_3O_4 to CoO transformation in these hydroxide-derived spinel phases occurs at lower temperatures compared with the reported data of 1000–1200 °C under air.[20,21] As revealed in XRD patterns, the crystallinity of the low-temperature formed Co_3O_4 is low, which may ease oxygen transport during phase conversion and result in the observed low transformation temperature.

Catalytic evaluation of the thermally formed Co_3O_4

Fig. 10 shows specific surface area data for some representative samples calcined at various temperatures for 2 h. As can be seen, brucite-like compounds, N5 and A1 (A1 contains a small amount of hydrotalcite-like phase), show higher specific surface area at low temperature (200 °C). However, they show

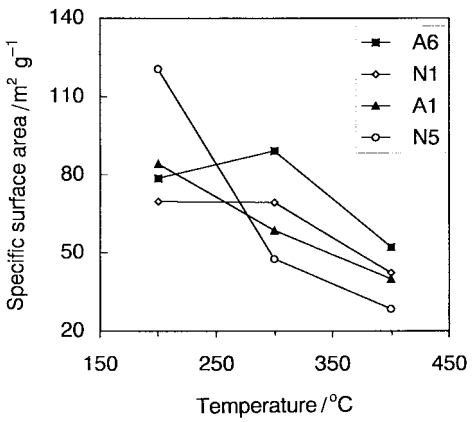

Fig. 10 Specific surface area *versus* calcination temperature for some representative Co hydroxide samples.

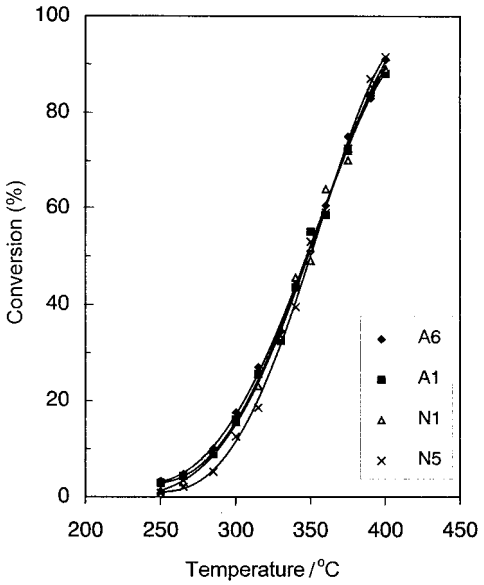

Fig. 11 Conversion *versus* temperature curves for some representative Co hydroxides calcined at 400 °C.

significantly reduced specific surface areas at elevated temperatures. On the other hand, the surface areas of hydrotalcite-like samples (N1 and A6) are systematically higher than those of N5 and A1 at 300 and 400 °C. In particular the surface areas of these high-temperature calcined samples are proportional to the anion content in the precursor compounds, *i.e.*, $S_{A6} > S_{N1} > S_{A1} > S_{N5}$ (see Table 2 for the anion content).

Fig. 11 shows the chemical reactivity of the above thermally formed samples using nitrous oxide as a probe gas at $\leqslant 400$ °C. These conversion *versus* temperature curves were obtained at a GHSV of 20 500 h^{-1}. Although they are prepared from various starting Co hydroxides, the 400 °C-formed oxides occur strictly as Co_3O_4 crystallographic phases,[30] as revealed by XRD before and after nitrous oxide decomposition. Owing to the same Co_3O_4 phase, the observed catalytic activity varies only slightly. Although surface area is usually critical in determining catalytic activity, a variation in specific surface area by a factor of *ca.* two has been shown to have little effect (N5 *versus* A6, Table 3). Therefore, the subtle differences among these curves can be attributed to a combined effect of total variation in specific surface area, number of reaction sites per specific surface area, and activity of a reaction site. Overall all Co_3O_4 oxides derived from these monohydroxides are highly active, when compared with the literature conversion data. For example, the activity of the present catalytic oxides at 375 °C is in the range 7.2–8.2 mmol N_2O g^{-1} h^{-1} (GHSV = 82 000 h^{-1}, N_2O = 1 mol% balanced with He), compared with 1.6–2.3 mmol N_2O g^{-1} h^{-1} (GHSV = 30 000 h^{-1}, N_2O = 0.1 mol% balanced with He) for an active hydrotalcite-like compound ($Co^{II}Mg^{II}Al^{III}$-HT) derived catalyst operated at 350–400 °C.[31,32]

As the decomposition reaction occurs on the surface, the actual crystallographic phase of surface Co_3O_4 should be further addressed. Using XPS, it is known that the transformation in eqn. (3) occurs at *ca.* 347 °C on the surface of Co_3O_4 in an oxygen atmosphere of 1×10^{-3} Pa, which is *ca.* 186 °C lower than for thermodynamic calculation for the bulk phase Co_3O_4 to CoO transition under the same P_{O_2}.[29] Since the oxygen partial pressure generated by the current nitrous oxide decomposition is much higher than 1×10^{-3} Pa (P_{O_2} = 4–16 Pa for the reactions 250 °C and 446–466 Pa at 400 °C reactions, Fig. 11), it is expected that the surface Co_3O_4 to CoO transition should occur at a temperature much higher than 347 °C (for $P_{O_2} = 1 \times 10^{-3}$ Pa) found in the XPS study;[21] *i.e.* nitrous oxide decomposition is largely carried out on the Co_3O_4 surface phase, rather than CoO.

Table 3 Kinetic data of nitrous oxide decomposition from some representative catalysts

Sample	Structural phase[a]	E_a/ kJ mol^{-1}	ln A	Specific surface area[b]/m^2 g^{-1}
N5	B(II)	94	19.5	29
A1	B(II)+HT(II,III)	80	16.7	40
N1	HT(II)	83	17.4	42
A6	HT(II,III)	79	16.8	52

[a]The phase notation is the same as in Table 1. [b]Upon calcination at 400 °C.

Decomposition of nitrous oxide on a metal oxide surface involves an electron transferring from a low-oxidation state metal cation to an adsorbed nitrous oxide molecule.[33,34] For many metal oxide catalysts, charge transfer from a low-valence metal cation to the adsorbed N_2O is often considered as a fast surface reaction. Based on this mechanism, a typical Langmuir–Hinshelwood rate equation can be derived.[15] In particular, the following simplified equation can be obtained considering the adsorption step as a controlling step and a negligible inhibiting role of O_2 in the decomposition reaction:[15,35,36]

$$-dP_{N_2O}/dt = kP_{N_2O} \quad (4)$$

After integration, eqn. (4) becomes:

$$\ln\{\ln(P_{i,N_2O}/P_{f,N_2O})\} = \ln A - \ln(F/V) - E_a/RT \quad (5)$$

where V and F have been defined in Experimental section, and A is Arrhenius pre-exponential factor, and E_a is the apparent activation energy of decomposition.[35] Eqn. (5) has been employed in the current work to provide a correlation between the preparative method and catalytic activity of Co_3O_4. Since the $\ln\{\ln(P_{i,N_2O}/P_{f,N_2O})\}$ *versus* $1/T$ plots are all fitted very well to straight lines, decomposition kinetics of nitrous oxide on these Co_3O_4 oxides can be described as first order with partial pressure of nitrous oxide with apparent activation energies of 79–94 kJ mol^{-1} as listed in Table 3, noting that these values are quite similar.

Conclusions

In summary, the synthetic chemistry and thermal evolution of one new and two known Co hydroxides have been investigated systematically with a wide range of characterisation and analytical methods (XRD/EA/DSC/FTIR/DTA/TGA/GC). Three major decomposition stages of Co hydroxides have been identified: (i) 149–164 °C for dehydration of interlayer water, (ii) 185–197 °C and (iii) 219–222 °C for dehydroxylation of hydrotalcite and brucite-like phases, respectively. Intercalated nitrate anions decompose largely at the stage (ii). During the above decomposition, Co_3O_4 oxide starts to form at temperatures as low as 165 °C especially for hydrotalcite-like phases. The intermediate compound $HCoO_2$, formed during the thermal evolution, decomposes at 258–270 °C. It is found that Co_3O_4 oxide formed freshly from thermal decomposition of the hydroxides coverts to CoO at 842–858 °C and 935–948 °C under nitrogen and air, respectively. Surface areas of calcined samples are found to be proportional to their intercalated anion content. The resultant Co_3O_4 materials are catalytically active and the activity is comparable to some reported active catalyst systems. For example, the activity of Co_3O_4 oxide operated at 375 °C is in the range 7.2–8.2 mmol N_2O g^{-1} h^{-1} (GHSV = 82 000 h^{-1}, N_2O = 1 mol% balanced with He).

The authors gratefully acknowledge research funding (RP960716) co-supported by the Ministry of Education and the National Science and Technology Board of Singapore.

References

1 D.L. Bish and A. Livingstone, *Miner. Mag*., 1981, **44**, 339.
2 C. Faure, C. Delmas and M. Fousassier, *J. Power Sources*, 1991, **35**, 279.
3 P. V. Kamath and N. Y. Vasanthacharya, *J. Appl. Electrochem*., 1992, **22**, 483.
4 P. Rabu, S. Angelov, P. Legoll, M. Belaiche and M. J. Drillon, *Inorg. Chem*., 1993, **32**, 2463.
5 P. Benard, J. P. Auffredic and D. Louer, *Thermochim. Acta*, 1994, **232**, 65.
6 A. Delahaya-Vidal, K. Tekaia Ehlsissen, P. Genin and M. Figlarz, *Eur. J. Solid State Inorg. Chem.*, 1994, **31**, 823.
7 P. V. Kamath, M. Dixit, L. Indira, A. K. Shukla, V. G. Kumar and N. Munichandraiah, *J. Electrochem. Soc*., 1994, **141**, 2956.
8 P. V. Kamath and G. H. A. Therese, *J. Solid State Chem*., 1997, **128**, 38.
9 F. Cavani, F. Trifiro and A. Vaccari, *Catal. Today*, 1991, **11**, 173.
10 W. T. Reichle, *Solid State Ionics*, 1986, **22**, 135.
11 H. C. Zeng, Z. P. Xu and M. Qian, *Chem. Mater*., 1998, **10**, 2277.
12 M. Qian and H. C. Zeng, *J. Mater. Chem*., 1997, **7**, 493.
13 L. V. Pyatnitskii, *Analytical Chemistry of Cobalt*, IPST (Israel Program for Scientific Translations), Jerusalem, 1966, p. 5.
14 F. Kapteijn, J. Rodriguez-Mirasol and J. A. Moulijn, *Appl. Catal. B*, 1996, **9**, 25.
15 K. Li, X. F. Wang and H. C. Zeng, *Chem. Eng. Res. Des. Part A: Trans. I. Chem. E*., 1997, **75**, 807.
16 X. F. Wang and H. C. Zeng, *Appl. Catal. B*, 1998, **17**, 89.
17 Powder Diffraction File, Card No. 45-0031. Joint Committee on Powder Diffraction Standards, Swarthmore, PA, 1995.
18 I. E. Grey and R. Ragozzini, *J. Solid State Chem*., 1991, **94**, 244.
19 M. A. Ulibarri, M. J. Hernandez and J. Cornejo, *J. Mater. Sci*., 1991, **26**, 1512.
20 M. Schraml-Marth, A. Wokaun and A. Baiker, *J. Catal*., 1992, **138**, 306.
21 J. M. Fernandez, C. Barriga, M. A. Ulibarri, F. M. Labajos and V. Rives, *J. Mater. Chem*., 1994, **4**, 1117.
22 I. C. Chisem and W. Jones, *J. Mater. Chem*., 1994, **4**, 1737.
23 S. Kannan and C. S. Swamy, *J. Mater. Sci. Lett.*, 1992, **11**, 1585.
24 G. Busca, F. Trifiro and A. Vaccari, *Langmuir*, 1990, **6**, 1440.
25 N. Zotov, K. Petrov and M. Dimitrova-Pankova, *J. Phys. Chem. Solids*, 1990, **51**, 1199.
26 E. Kruissink, L. L. van Reijen and J. R. H. Ross, *J. Chem. Soc., Faraday Trans. 1*, 1981, **77**, 649.
27 *Handbook of Chemistry and Physics*, ed. D. R. Lide, CRC Press, USA, 78th edn., 1997, p. 5.
28 K. Shigeharu, N. Uchida, I. Miyashita and T. Wakayama, *Colloids Surf.*, 1989, **37**, 39.
29 M. Oku and Y. Sato, *Appl. Surf. Sci.*, 1992, **55**, 37.
30 Powder Diffraction File, Card No. 9-418. Joint Committee on Powder Diffraction Standards, Swarthmore, PA, 1967.
31 S. Kannan and C. S. Swamy, *Appl. Catal. B*, 1994, **3**, 109.
32 J. N. Armor, T. A. Braymer, T. S. Farris, Y. Li, F. P. Petrocelli, E. L. Weist, S. Kannan and C. S. Swamy, *Appl. Catal. B*, 1996, **7**, 397.
33 S. Akbar and R. W. Joyner, *J. Chem. Soc., Faraday Trans. 1*, 1981, **77**, 803.
34 D. D. Eley, A. H. Klepping and P. B. Moore, *J. Chem. Soc., Faraday Trans. 1*, 1985, **81**, 2981.
35 R. Sundararajan and V. Srinivasan, *Appl. Catal*., 1991, **73**, 165.
36 A. Cimino, *Chim. Ind.* (*Milan*), 1974, **56**, 27.

Paper 8/04767G